algorithms make the determination of 3-D inter-frame motion a simple task.

Extensive experiments have been conducted to characterise the performance of the algorithms with both synthetic and real image data. Experimental results have clearly demonstrated the validity of the algorithms and the benefits of making full use of data redundancy.

8 References

[1] H. Weyl, Symmetry, Princeton University Press, 1952.

[2] M. Enquist and A. Arak, Symmetry, Beauty and Evolution, Nature, vol.372, 1994, pp.169-172.

[3] T. Kanade, Recovery of the Three-Dimensional Shape of an Object from a Single View, Artificial Intelligence, vol.17, 1981, pp.409-460.

[4] A. D. Gross and T. E. Boult, Analysing Skewed Symmetries, Int. J. Computer Vision, vol.13, 1994, pp.91-111.

[5] P. L. Palmer, M. Petrou and J. Kittler, An Optimisation Approach to Improve the Accuracy of the Hough Transform - Plane Orientations from Skewed Symmetry, Proc. of CVPR93, pp.682-683.

[6] T. J. Cham and R. Cipolla, Geometric Saliency of Curve Correspondences and Grouping of Symmetric Contours, Proc. of ECCV96, vol.I, 1996, pp.385-398.

[7] F. Ulupinar and R. Nevatia, Constraints for Interpretation of Line Drawings Under Perspective Projection, CVGIP: Image Understanding, vol.53, 1991, pp.88-96.

[8] H. Mitsumoto, et. al., 3-D Reconstruction Using Mirror Images Based on a Plane Symmetry Recovering Method, IEEE Trans. PAMI, vol.14, 1992, pp.941-946.

[9] R. Glachet, J. T. Lapreste and M. Dhome, Locating and Modelling a Flat Symmetric Object from a Single Perspective Image, CVGIP: Image Understanding, vol.57, 1993, pp.219-226.

[10] C. A. Rothwell et. al., Extracting Projective Structure from Single Perspective Views of 3-D Point Sets, *Proc. of 4th ICCV*, Berlin, Germany, 1993, pp.573-582.

[11] T. N. Tan, Structure, Pose and Motion of Bilateral Symmetric Objects, Proc. of 6th British Mach. Vision Conf., Birmingham, England, 1995, pp.473-482.

[12] C. I. Attwood, G. D. Sullivan and K. D. Baker, Model Construction from a Single Perspective View Using Shape from Symmetry, Proc. of BMVC93, 1993, pp.155-164.

[13] T. S. Huang and A. N. Netravali, Motion and Structure from Feature Correspondences: A Review, Proc. of IEEE, vol.82, 1994, pp.252-268.

[14] K. Arun, T. S. Huang and S. Blostein, Least Squares Fitting of Two 3-D Point Sets, IEEE Trans. PAMI, vol.9, 1987, pp.698-700.

[15] B. Horn, Closed-form Solution of Absolute Orientation Using Unit Quaternion, J. Opt. Soc. Am. A, vol.4, 1987, pp.629-642.

easily be measured. The recovered dimensions from the four views are listed in Table 2. In spite of non-perfect bilateral symmetry of the sponge, the recovered structure in each view is very accurate.

Table 2 : Recovered dimensions (in mm) of the sponge sequence (Fig.8)

Distance	Truth	Fig.8(a)	Fig.8(b)	Fig.8(c)	Fig.8(d)
P_1Q_1	113.00	113.00	113.00	113.00	113.00
P_2Q_2	151.00	150.98	149.14	152.18	151.14
P_3Q_3	60.00	57.98	58.24	60.61	57.62
P_1P_2	62.00	61.02	62.12	63.25	61.59
P_2P_3	84.00	83.28	82.09	87.14	84.02
Ave. Error (%)	**0.00**	**1.16**	**1.33**	**1.51**	**0.99**

6.3 Results of 3-D motion estimation

The 3-D motion estimation algorithm outlined in Section 5 was tested with the images shown in Figures 6-8. In each case, one of the views was chosen as the reference frame and the absolute orientation technique of Horn [15] was applied to determine the 3-D motion between the reference frame and each of the other frames. The reference frames for the three image sequences are respectively Fig.6(a), Fig.7(a) and Fig.8(a).

Since true motion parameters were unknown, the following procedure was adopted to assess, indirectly, the accuracy of the recovered motion. For each sequence the camera coordinates of all points in all frames (except the reference frame of course) were predicted based on the recovered motion and the recovered camera coordinates of the same points in the reference frame. Image positions of all points in all frames were reconstructed from the predicted coordinates. The reconstructed positions were then compared with the original image positions. The results are shown in Table 3. In all cases, the average absolute error (distance) between the original and the reconstructed image positions is around 1 pixel, indicating a good level of accuracy of the recovered motion parameters.

Table 3 : Errors (in pixels) between original and motion-reconstructed image points

Motion	Fig6(a) to Fig.6(b)	Fig.6(a) to Fig.6(c)	Fig.7(a) to Fig.7(b)	Fig.7(a) to Fig.7(c)	Fig.8(a) to Fig.8(b)	Fig.8(a) to Fig.8(c)	Fig.8(a) to Fig.8(d)
Ave. Error	0.54	0.82	0.97	0.89	1.11	1.30	0.62

7 Conclusions

Several novel algorithms have been described for recovering the range parameters of bilateral symmetric objects using single perspective views. Unlike many existing algorithms, the new algorithms do not rely on the error-prone process of vanishing point detection. Particular attention has been given to the maximum exploitation of data redundancy for the sake of noise robustness. It has been shown that the range recovery

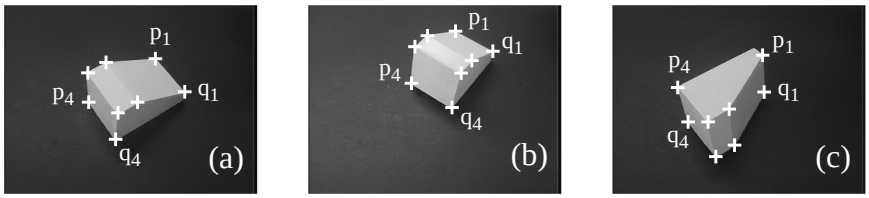

Figure 7: Three images of a block sequence. +s indicate the corner points used in range recovery.

Table 1. The true dimensions were measured by hand and therefore subject to some measurement errors. Again the recovered structure tallies well with the measured ones, with average relative range errors no greater than 2.5%.

Table 1 : Recovered dimensions (in mm) of the block sequence (Fig.7)

Distance	**Truth**	**Fig.7(a)**	**Fig.7(b)**	**Fig.7(c)**
P_1Q_1	73.00	73.00	73.00	73.00
P_2Q_2	73.00	74.27	74.76	73.38
P_3Q_3	73.00	73.03	74.7	72.98
P_4Q_4	73.00	71.42	73.71	76.31
P_1P_2	107.00	109.54	105.6	109.96
P_2P_3	31.00	29.25	33.59	31.21
P_3P_4	76.00	72.03	75.17	77.53
Ave. Error (%)	**0.00**	**2.45**	**2.35**	**1.50**

The last example deals with a more complicated bilateral symmetric object. It is a sponge used in packaging. Four views of the sponge are shown in Fig.8. Because of the

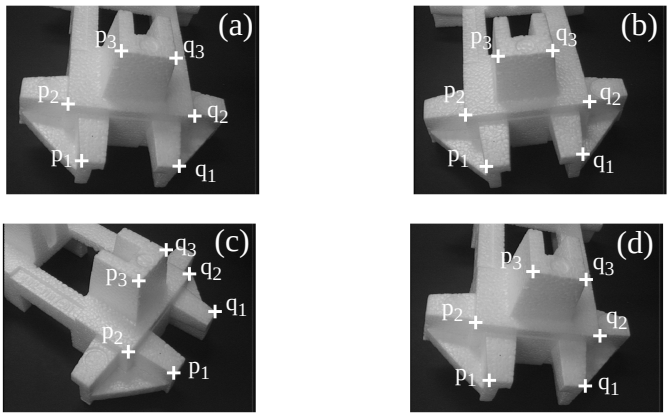

Figure 8: Four images of a sponge sequence. +s indicate the corner points used in range recovery.

difficulties in measuring distances, only three point pairs were used whose distances can

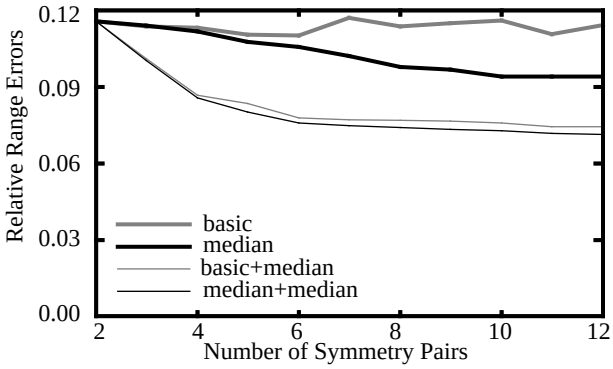

Figure 5: Effect of more points on the performance of the basic algorithm (thick grey), the median algorithm (thick dark), the basic algorithm enhanced with median midpoints (thin grey), and the median algorithm enhanced

algorithm becomes clearer with more points.

6.2 Range recovery of real objects

The algorithms were also applied to a number of real bilateral symmetric objects found in our lab. Three examples are reported here to illustrate the typical performances of the algorithms. The results given were obtained by the median algorithm but those by other algorithms were not significantly different. The corner points were found by the Plessey corner finder, and if the corner finder failed to locate a particular corner, the corner was then identified by eye. The symmetric correspondences between the located corner points were established manually (the automatic identification of symmetric points is a non-trivial problem and is beyond the scope of the current paper).

The first example shown in Fig.6 deals with a planar object. The "tree" was first hand-drawn and printed on paper. The printed version was then captured at three different

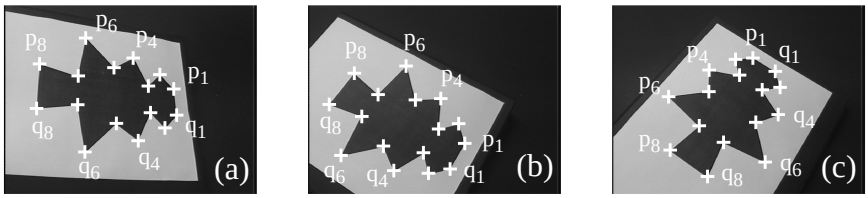

Figure 6: Three images of a "tree" sequence. +s indicate the corner points used in range recovery.

locations. The corner points used are indicated by +s. The true and recovered dimensions (lengths of line segments connecting the corner points) of the tree were compared and the average relative error was calculated for each location. The results for Fig.6(a)-(c) are 3.04%, 2.41% and 4.28% respectively. As a whole, the recovered structure is fairly accurate and the average relative error does not exceed 5%.

The second example is a bilateral symmetric block. Four symmetric pairs were located in three views as shown in Fig.7. The recovered dimensions are summarised in

compare the performance of the various range recovery algorithms, whereas a number of real objects were used to illustrate the performance of the algorithms with typical practical data. This section reports the results of these experiments.

6.1 Range recovery of synthetic data

Synthetic data were generated by randomly selecting a specified number of pairs of bilateral symmetric points within a cuboid using known camera parameters. Error in low-level image processing was simulated by perturbing the ideal image coordinates of each point by a random value ω uniformly distributed in $[-\Omega, \Omega]$ (in pixels). Ω indicates the level of noise. All images were of size 768x575 pixels.

The number of symmetric point pairs was first fixed at $N = 6$ and extensive Monte Carlo simulations were conducted to investigate the effect of increasing noise level on the accuracy of the recovered range parameters. The results of the simulations are summarised in Fig.4. A number of interesting observations can be made from Fig.4:

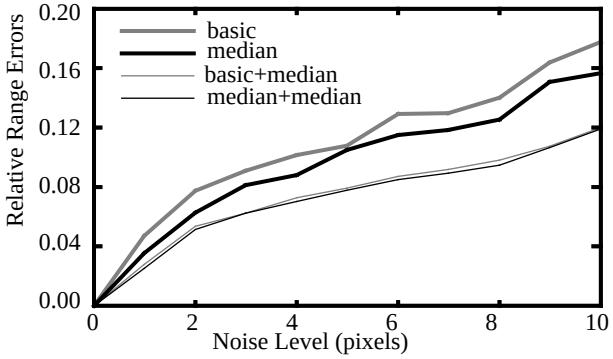

Figure 4: Noise performance of the basic algorithm (thick grey), the median algorithm (thick dark), the basic algorithm enhanced with median midpoints (thin grey), and the median algorithm enhanced with median midpoints (thin dark).

- None of the algorithms has a relative range error greater than 20%, even under the unrealistically high noise level of $\Omega = 10$.
- The localisation of midpoints based on median operations (Equation (11)) greatly improves the performance of the basic and the median algorithm.
- As expected, the median algorithm always outperforms the basic algorithm, though the difference is barely noticeable when both algorithms are enhanced with median midpoints.
- When computational cost is at a premium, the basic algorithm enhanced with median midpoints seems to be the best choice.

A second set of Monte Carlo simulations was conducted to see how the performance of the algorithms may be improved by using more points. The results are plotted in Fig.5. As expected, the performance of the basic algorithm is essentially unaffected by the increasing number of points since the algorithm treats each pair independently. On the other hand, that of the other algorithms all has noticeably been improved with more points (though the improvement tends to saturate beyond 6-8 point pairs). The other interesting observation from Fig.5 is that the advantage of the median algorithm over the basic

accuracy of the located midpoints has a significant effect on that of the reconstructed object. For a symmetric trapezium formed by two given pairs of symmetric points, the basic and the median algorithm locate the two projected midpoints only by using the image coordinates of the four corners of the corresponding trapezium, making no use of data associated with other points.

This is rectified by the following to achieve further exploitation of data redundancy. To determine the projected midpoint m_1 of the first symmetry line P_1Q_1, we consider the $N-1$ trapezia the symmetry line forms with each of the remaining $N-1$ pairs. For each trapezium, we locate m_1 according to Fig.2(b). This produces a list of $N-1$ candidate positions for m_1, all lying on the image line segment p_1q_1:

$$\{m_1^{(i)};\quad i=1,2,...,N-1\} \tag{10}$$

where the superscript (i) indicates the image position determined in the i^{th} trapezium. For the sake of noise robustness, the final solution for m_1 is determined by the following median operation:

$$m_1 = \textbf{median}\{m_1^{(i)};\quad i=1,2,...,N-1\} \tag{11}$$

The projected midpoints of other symmetry lines are determined similarly. The image coordinates of the midpoints so recovered can then be used by the basic and the median algorithm.

5 Determination of inter-frame motion

The previous sections show that bilateral symmetry can be exploited to facilitate 3-D monocular reconstruction. Bilateral symmetry also greatly simplifies the determination of 3-D inter-frame motion. Let us consider the recovery of the 3-D motion of a bilateral symmetric object between two frames. We assume known intra-frame symmetric correspondences and inter-frame point correspondences. The problem is the well-known structure-from-motion (SFM) problem and may be solved using one of the many existing methods [13].

Here we show that by using the algorithms presented in the previous sections, the 3-D motion of a bilateral symmetric object can be determined in a very simple and efficient way, and closed-form solutions only require a minimum of two symmetric point pairs. For each view, the algorithms of the previous sections are employed to recover the range parameters of all points. The determined range parameters are then used to compute the 3-D camera coordinates of the points (using Equation (2)). The global scale in each frame may be resolved by assuming the same length (e.g., unit length) of the same symmetry line so as to ensure consistent inter-frame scale. At the end of this process, we obtain a set of 3-D to 3-D point correspondences with known camera coordinates. The 3-D inter-frame motion can then easily be determined by using one of the standard absolute orientation algorithms. Several of these algorithms, e.g., Arun, Huang and Blostein [14], and Horn [15], provide efficient closed-form solutions.

6 Experimental results

A large set of experiments were carried out to characterise the performance of the algorithms described in the previous sections. Synthetic data were used to quantify and

simple straightforward extension of the trapezium algorithm outlined in the preceding section to algorithms which take full advantage of data redundancy for the sake of noise robustness.

4.1 The basic algorithm

For an object with N pairs of bilateral symmetric points $\{P_i, Q_i;\ \ i=1,2,...,N\}$, any two pairs $\{P_i, Q_i\}$ and $\{P_j, Q_j\}$ $(i \neq j)$ form a symmetric trapezium. To determine the ranges of the $2N$ points, we consider the $N-1$ trapezia formed by the first pair $\{P_1, Q_1\}$ and each of the remaining $N-1$ pairs $\{P_i, Q_i;\ \ i=2,...,N\}$. For each trapezium, we recover its ranges using the trapezium reconstruction algorithm outlined in the previous section. This way the first pair $\{P_1, Q_1\}$ is used as the reference pair and the ranges of all points are recovered up to a common global scale.

4.2 The median algorithm

Although simple, the basic algorithm has a problem with noisy data. Since the first pair is directly involved in the recovery of all points, the successful reconstruction of the overall object is overly dependent on the accuracy of the data associated with the first pair. This is clearly undesirable. Without any *a priori* knowledge, there is no reason to favour the first pair over other pairs.

The bias towards the first pair is eliminated by applying the basic algorithm N times, each time with a different reference pair. This process generates N sets of range parameters:

$$\{\lambda_{P_1}^{(i)}, \lambda_{Q_1}^{(i)}, \lambda_{P_2}^{(i)}, \lambda_{Q_2}^{(i)}, \ldots, \lambda_{P_N}^{(i)}, \lambda_{Q_N}^{(i)};\ \ i=1,2,...,N\} \tag{7}$$

where the superscript (i) indicates the range parameters determined using the i^{th} pair as the reference pair. Because the reference pairs are different, each set of range parameters in Equation (7) is in general subject to a different global scale. The N sets can be brought to the same global scale by setting the range of one of the points to a common value (say 1.0). This may be achieved, for example, by dividing the ranges of each set by that of the first point. We denote the N sets of normalised range parameters as

$$\{\bar{\lambda}_{P_1}^{(i)}, \bar{\lambda}_{Q_1}^{(i)}, \bar{\lambda}_{P_2}^{(i)}, \bar{\lambda}_{Q_2}^{(i)}, \ldots, \bar{\lambda}_{P_N}^{(i)}, \bar{\lambda}_{Q_N}^{(i)};\ \ i=1,2,...,N\} \tag{8}$$

Under noise-free conditions, the N normalised sets should be identical since they describe the normalised structure of the same object. When data is contaminated by noise, however, this is no longer true. The final set of range parameters is determined by the following median operations:

$$\lambda_{P_j} = \mathbf{median}\{\bar{\lambda}_{P_j}^{(i)};\ \ i=1,2,...,N\};\ \ \lambda_{Q_j} = \mathbf{median}\{\bar{\lambda}_{P_j}^{(i)};\ \ i=1,2,...,N\} \tag{9}$$

The global scaling factor in the recovered range parameters may be resolved by knowing the absolute range of one of the points, or the length of one of the symmetry lines, or any other equivalent absolute information.

4.3 Robust localisation of midpoints

The performance of the median algorithm can be further improved by making additional use of data redundancy. A central step in the basic algorithm and hence the median algorithm is the localisation of the projected midpoints of the symmetry lines. The

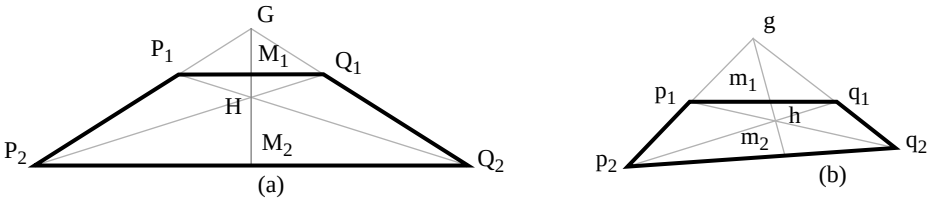

Figure 2: Labelling of a bilateral symmetric trapezium (a) and its image (b).

image positions of the four corners of a symmetric trapezium, the image positions of the two midpoints can be determined according to Fig.2(b).

To determine the ranges of the four corners and the two midpoints of the trapezium, we consider the triangle $\Delta P_1 O Q_1$ on the interpretation plane defined by the focal point O and the image points p_1 and q_1 (see Fig.3). The similarity of the two triangles

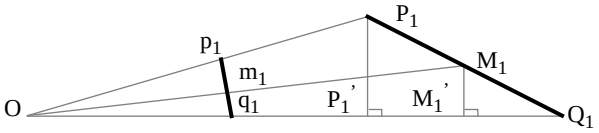

Figure 3: Triangles on an interpretation plane.

$\Delta P_1 P_1' Q_1$ and $\Delta M_1 M_1' Q_1$ leads to the following (see [11] for derivation):

$$\lambda_{P_1} = \frac{2\sqrt{1-(\boldsymbol{q}_1 \cdot \boldsymbol{m}_1)^2}}{\sqrt{1-(\boldsymbol{p}_1 \cdot \boldsymbol{q}_1)^2}} \lambda_{M_1} \equiv W_{P_1} \lambda_{M_1}; \quad \lambda_{Q_1} = \frac{2\sqrt{1-(\boldsymbol{p}_1 \cdot \boldsymbol{m}_1)^2}}{\sqrt{1-(\boldsymbol{p}_1 \cdot \boldsymbol{q}_1)^2}} \lambda_{M_1} \equiv W_{Q_1} \lambda_{M_1} \quad (3)$$

By considering the triangle $\Delta P_2 O Q_2$ and following the same procedure, we obtain similar expressions for λ_{P_2} and λ_{Q_2}:

$$\lambda_{P_2} = \frac{2\sqrt{1-(\boldsymbol{q}_2 \cdot \boldsymbol{m}_2)^2}}{\sqrt{1-(\boldsymbol{p}_2 \cdot \boldsymbol{q}_2)^2}} \lambda_{M_2} \equiv W_{P_2} \lambda_{M_2}; \quad \lambda_{Q_2} = \frac{2\sqrt{1-(\boldsymbol{p}_2 \cdot \boldsymbol{m}_2)^2}}{\sqrt{1-(\boldsymbol{p}_2 \cdot \boldsymbol{q}_2)^2}} \lambda_{M_2} \equiv W_{Q_2} \lambda_{M_2} \quad (4)$$

From the fact that the line connecting the two midpoints is perpendicular to the symmetry lines, we can relate λ_{M_1} and λ_{M_2} to each other [11]:

$$\lambda_{M_1} = \frac{W_{P_1}(\boldsymbol{p}_1 \cdot \boldsymbol{m}_2) - W_{Q_1}(\boldsymbol{q}_1 \cdot \boldsymbol{m}_2)}{W_{P_1}(\boldsymbol{p}_1 \cdot \boldsymbol{m}_1) - W_{Q_1}(\boldsymbol{q}_1 \cdot \boldsymbol{m}_1)} \lambda_{M_2} \equiv W \lambda_{M_2} \quad (5)$$

Equations (3)-(5) simply indicate that the ranges of the trapezium can be recovered up to a global scale as summarised in the following:

$$\begin{aligned} \lambda_{P_1} &= W_{P_1} W \lambda_{M_2}; \ \lambda_{Q_1} = W_{Q_1} W \lambda_{M_2}; \\ \lambda_{P_2} &= W_{P_2} \lambda_{M_2}; \ \lambda_{Q_2} = W_{Q_2} \lambda_{M_2}; \lambda_{M_1} = W \lambda_{M_2} \end{aligned} \quad (6)$$

4 Reconstruction of general objects

We now turn our attention to the determination of the range parameters of points on a general bilateral symmetric object. Several algorithms are described, ranging from the

Ulupinar and Nevatia [7], Mitsumoto et. al. [8], Glachet et. al. [9], and Rothwell et. al. [10]. Most of these approaches use the *vanishing point* (VP) of the symmetry lines.

The detection of VPs in a single image is notoriously unstable unless the perspective distortion is severe. A non-VP-based approach is therefore preferred in practice. In our previous work [11], we described a simple algorithm for reconstructing bilateral symmetric trapezia from their perspective projections (image quadrilaterals). The algorithm does not involve direct computation of VPs. In this paper we extend the trapezium algorithm of [11] to more general 2-D and 3-D bilateral symmetric objects. Several novel algorithms are described and extensive experiments are reported. The algorithms presented here will prove useful for interactive construction of 3-D geometric models of objects such as vehicles [12].

2 Imaging geometry and notations

The imaging geometry assumed in this paper is depicted in Fig.1. The origin of the camera

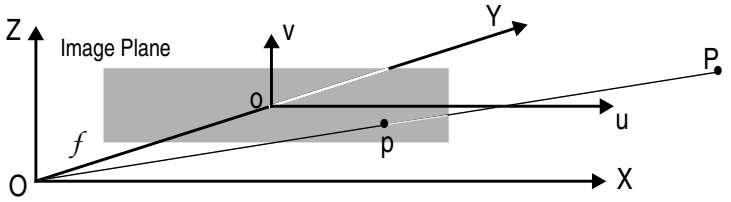

Figure 1: Illustration of imaging geometry.

coordinate system (CCS) is the focal point. The optical axis of the camera is aligned with the Y-axis of the CCS. The image plane is at a known distance f in front of the focal point and is orthogonal to the optical axis. The abscissa axis (the u-axis) of the image plane is parallel to the X-axis and the ordinate axis (the v-axis) to the Z-axis.

For a given 3-D point P, we use $\boldsymbol{P}$ to represent its camera coordinates, $p = (u, v)$ its image position, and $\boldsymbol{p}$ the unit direction vector from the focal point O to the image point p. Under the imaging geometry shown in Fig.1, the unit vector is given by

$$\boldsymbol{p} = \frac{1}{\sqrt{u^2 + f^2 + v^2}}(u \;\; \mathrm{f} \;\; \mathrm{v})^T \tag{1}$$

and the camera coordinates by

$$\boldsymbol{P} = \lambda_P \boldsymbol{p} \tag{2}$$

where λ_P is the range of P (the distance from the focal point O to P). The symmetrical point of P is denoted by Q, and the counterparts of $\boldsymbol{P}$, p, $\boldsymbol{p}$ and λ_P by $\boldsymbol{Q}$, q, $\boldsymbol{q}$ and λ_Q respectively. The midpoint of the symmetry line PQ is indicated by M, and its camera coordinates, image-plane position, unit direction vector and range by $\boldsymbol{M}$, m, $\boldsymbol{m}$ and λ_M.

3 Trapezium reconstruction

A symmetric trapezium and its perspective image are labelled as shown in Fig.2. By construction, image points m_1 and m_2 of Fig.2(b) are the perspective projections of the midpoints M_1 and M_2 of the two symmetry lines P_1Q_1 and P_2Q_2. Thus given the

Monocular Reconstruction of 3-D Bilateral Symmetrical Objects

T. N. Tan
Department of Computer Science
The University of Reading, Berkshire RG6 6AY, UK
Email: T.Tan@reading.ac.uk

Abstract

This paper concerns the 3-D monocular reconstruction of general bilateral symmetrical objects from a single perspective view. Bilateral symmetry is also exploited to simplify the estimation of 3-D inter-frame motion of such objects. Particular attention is given to the maximum exploitation of data redundancy for the sake of noise robustness. Several novel algorithms are described for recovering the range parameters of object points from their image coordinates in a single perspective view. The algorithms allow the 3-D inter-frame motion to be computed using well-known closed-form absolute orientation techniques. Experimental results with synthetic and a number of real objects are included to demonstrate the performance of the algorithms.

1 Introduction

Shape symmetry can be found in many objects [1]. Symmetry provides strong cues for human visual perception [2]. This paper concerns what is probably the most common form of symmetry - bilateral symmetry, which is also called reflectional or mirror symmetry. In this paper the lines connecting the bilateral symmetric points are termed as *symmetry lines*. For perfect bilateral symmetry, the midpoints of all symmetry lines lie on the same line (called the *symmetry axis* for 2-D objects) or the same plane (called the *symmetry plane* for 3-D objects). Symmetry lines are parallel to each other, and are perpendicular to the symmetry axis or plane.

The nature of projection determines whether the midpoints, parallelism and perpendicularity of the symmetry lines are preserved or not after the 3-D to 2-D projection. If the projection is orthographic, midpoints and parallelism remain true but perpendicularity is lost. This gives rise to the so-called *skewed symmetry*. The most difficult case is full perspective projection which invalidates both the midpoints, parallelism and perpendicularity. In this case the projected symmetry lines intersect at a common point (the *vanishing point*) on the image plane. For convenience, we call the perspective projection of 3-D bilateral symmetry *perspective symmetry*.

Symmetry has been an active research area in the computer vision community for the past two decades or so. A plethora of approaches have been reported in the context of skewed symmetry analysis (e.g., [3-6]). These approaches assume (scaled) orthographic projection, and typically focus on the detection of the symmetry axis of 2-D bilateral symmetric shapes on the image plane. In contrast, work on perspective symmetry analysis has been very limited indeed. The best-known published work in the area includes